Time-Dependent Two-Layer Hydraulic Exchange Flows*

KARL R. HELFRICH

Department of Physical Oceanography, Woods Hole Oceanographic Institution, Woods Hole, Massachusetts

(Manuscript received 15 September 1993, in final form 18 July 1994)

ABSTRACT

A theory is presented for time-dependent two-layer hydraulic flows through straits. The theory is used to study exchange flows forced by a periodic barotropic (tidal) flow. For a given strait geometry the resulting flow is a function of two nondimensional parameters, $\gamma = (g'H)^{1/2}T/L$ and $q_{b0} = u_{b0}/(g'H)^{1/2}$. Here g', H, L, T, and u_{b0} are, respectively, the reduced gravity, strait depth and length scales, the forcing period, and the barotropic velocity amplitude; γ is a measure of the dynamic length of the strait and q_{b0} a measure of the forcing strength. Numerical solutions for both a pure contraction and an offset sill–narrows combination show that the exchange flow, averaged over a tidal cycle, increases with q_{b0} for a fixed γ. For fixed q_{b0} the exchange increases with increasing γ. The maximum exchange is obtained in the quasi-steady limit $\gamma \to \infty$. The minimum exchange is found for $\gamma \to 0$ and is equal to the unforced steady exchange. The usual concept of hydraulic control occurs only in these two limits of γ. In the time-dependent regime complete information on the strait geometry, not just at a finite number of control points, is required to determine the exchange. The model results are compared to laboratory experiments for the pure contraction case. Good agreement for both interface evolution and average exchange is found if account is made for the role of mixing, which acts to reduce the average salt (density) transport.

The relevance of these results to ocean straits is discussed. It is shown that many typical straits lie in the region of parameter space where time dependence is important. Application to the Strait of Gibraltar helps explain the success of the unforced steady hydraulic theory.

1. Introduction

Analysis of two-layer exchange flows through straits and over sills has traditionally relied on steady hydraulic theory. Recent advances in this area have been made by Armi (1986), Armi and Farmer (1986, hereafter AF), and Farmer and Armi (1986, hereafter FA). As in one-layer flow, control of the exchange between two basins can be exerted by contractions and sills. At the control locations the internal Froude number G,

$$G^2 = \frac{u_1^2}{g'h_1} + \frac{u_2^2}{g'h_2}, \qquad (1)$$

is critical, $G = 1$. Here u_i is the velocity and h_i is the depth in the upper ($i = 1$) and lower ($i = 2$) layers, $g' = (\rho_2 - \rho_1)/\rho_2$ is the reduced gravity, g is the acceleration due to gravity, and ρ_i is the layer density. Both AF and FA discuss the details of exchange flows for several different geometries. For both a pure contraction and a laterally offset sill–narrows combination the maximal exchange is achieved when there are two control points separated by a subcritical region ($G < 1$). This interior is isolated from the basins by supercritical ($G > 1$) exit regions. For a pure contraction with no net barotropic flow the two control points coalesce at the narrows. These maximal exchange solutions are the only solutions that can be matched to infinite basins where the depth of the layer exiting the strait goes to zero.

The application of the two-layer hydraulic theory to oceanographic situations has been reasonably successful. In the case of the Strait of Gibraltar dominant features of the flow such as control points and transitions from sub- to supercritical flow (hydraulic jumps) are often well represented (Armi and Farmer 1988; Farmer and Armi 1988). Bryden and Kinder (1990) showed that the steady theory compared well with the observed average transport through the strait.

There are, however, potential problems with the application of steady hydraulics. The most obvious is that it is often applied in situations that are time dependent. Many straits, including Gibraltar, are subject to strong barotropic tidal flows. At Gibraltar these flows are large enough to periodically reverse the flow of the lower layer over the sill (Camarinal Sill) from the direction predicted by the steady theory (Armi and Farmer 1988; Farmer and Armi 1988). Bryden et al. (1994) show that the unsteady average layer transport, $\overline{u_i'h_i'}$ (the

* Woods Hole Oceanographic Institution Contribution Number 8528.

Corresponding author address: Dr. Karl R. Helfrich, Department of Physical Oceanography, Woods Hole Oceanographic Institution, Woods Hole, MA 02543.

primes signify departures from the time mean), contributes about one-half of the total average transport $\overline{u_i h_i}$. Because the dynamics are fundamentally nonlinear it seems surprising that the steady theory employing average values works so well at Gibraltar.

The question then arises as to when time dependence modifies the dynamics so that the unforced steady model fails. Armi and Farmer (1986) proposed using a quasi-steady approximation in which the steady solutions, with $G = 1$ at the controls, apply at each point of the tidal forcing cycle. Time (through the barotropic flow) is simply a parameter of the problem. An average exchange, now a function of the barotropic forcing amplitude, can still be found. However, if either the time for long internal waves to propagate through the strait is the same order or longer than the timescale of the barotropic flow or if the temporal accelerations ($\partial u/\partial t$) are not small compared to the convective accelerations ($u\partial u/\partial x$), then the quasi-steady approximation is suspect. In these situations is the average exchange increased or decreased when compared to the quasi-steady result? How does the average exchange depend on the geometric and forcing (strength and frequency) parameters?

There have been relatively few studies of two-layer exchange flows with time-dependent forcing. Stigebrandt (1977) formulated a simple quasi-steady theory similar to AF's for exchange through a contraction and compared it with laboratory experiments. These results are rather limited since they were performed for an effectively zero length strait where the quasi-steady theory is expected to be valid. Wang (1989) conducted a numerical study of tidal flow on the exchange in the Strait of Gibraltar. He used a three-dimensional hydrostatic primitive equation model. His results were consistent with the observations and conclusions of Bryden and Kinder (1990) and Bryden et al. (1994). However, because of the model complexity and that only the Gibraltar case was studied, no conclusions about the general applicability of steady and quasi-steady hydraulic theory could be drawn. Geyer (1990) solved the time-dependent two-layer hydraulic equations for flow over a sill. His calculations clearly showed that with a strong oscillatory barotropic current the quasi-steady theory was invalid in all but a very short portion of the tidal cycle. However, since he imposed the magnitude of the exchange flow, the effect of the barotropic forcing on the exchange could not be investigated.

In this paper, the time-dependent dynamics of two-layer exchange flows with an imposed barotropic tidal flow is examined. The goal is to determine how the average exchange is modified by the forcing characteristics and the strait geometry and the parametric regions of validity of the unforced steady and forced quasi-steady hydraulic theories. In section 2, a time-dependent two-layer hydraulic model is developed, which shows that for a given strait geometry the exchange flow depends on just two nondimensional parameters. One is a measure of the importance of time dependence and the second is a measure of the forcing strength. In section 3, the model is solved for the a pure contraction and for a laterally offset sill and contraction. In both situations the exchange flow is not specified but is a result of the calculation. Section 4 discusses the results of laboratory experiments for the pure contraction. The experiments support the model but highlight the role of mixing. A discussion of the results and applications to oceanic straits is given in section 5.

2. The model

The model is based on two-layer hydrostatic flow through a strait separating two infinite basins. Rotation is not considered; therefore, the model is limited to straits that are much narrower than the internal Rossby radius of deformation. A sketch of the model geometry is given in Fig. 1. The assumption of slow variations in both strait width $b(x)$ and depth result in the following nondimensional momentum

$$\frac{\partial u_i}{\partial t} + \frac{\partial}{\partial x}\left[\frac{u_i^2}{2} + (1 - i)h_1 + \frac{1}{\sigma}(h_1 + h_2 - h_s)\right] = 0 \qquad (2a,b)$$

and continuity

$$\frac{\partial a_i}{\partial t} + \frac{\partial}{\partial x}(a_i u_i) = 0 \qquad (3a,b)$$

equations for each layer ($i = 1, 2$). Here u_i, h_i, and

$$a_i = b(x)h_i \qquad (4)$$

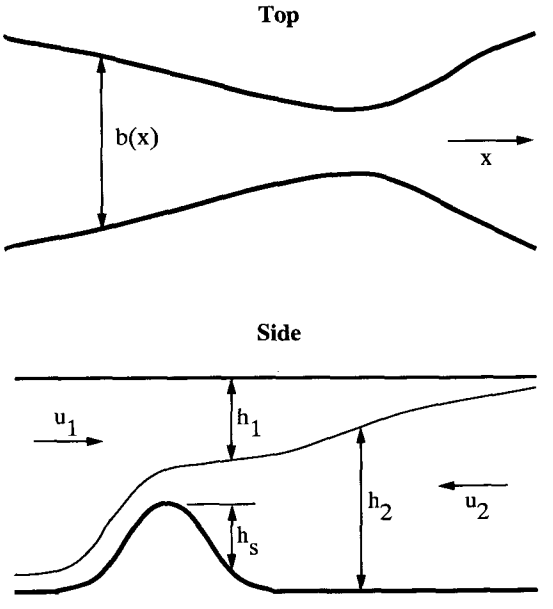

FIG. 1. Definition sketch.

are the velocity, depth, and area, respectively, of the upper ($i = 1$) and lower ($i = 2$) layers. The depth of the bottom below the sill crest is $h_s(x)$, $\sigma = (\rho_2 - \rho_1)/\rho_2$ is the layer density difference, x is the alongstrait dimension, and t is time. Equations (2a,b) and (3a,b) have been normalized with $(g'H)^{1/2}$ for u_i, H for h_i and x, $(H/g')^{1/2}$ for t, and $A_0 = b_0 H$ for a_i. Here $g' = g\sigma$, b_0 is the strait width at the sill (at the narrows if no sill is present), and H is the total undisturbed depth over the sill. In (2a,b) it is assumed that the pressure on the free surface is zero. This term can be retained, but in what follows it would eventually be eliminated.

In the Boussinesq limit, $\sigma \ll 1$, the rigid-lid approximation is valid and

$$h_1 + h_2 = 1 + h_s. \tag{5}$$

The barotropic transport q_b is then a function of time only,

$$q_b(t) = u_1 a_1 + u_2 a_2, \tag{6}$$

and must be specified. Equations (2a,b) and (3a,b) can then be reduced to two equations in two unknowns, a_1 and the shear

$$U = u_2 - u_1.$$

The resulting equations are

$$\frac{\partial a_1}{\partial t} + \frac{\partial}{\partial x}\left[\frac{a_1 q_b + U a_1^2}{A} - U a_1\right] = 0 \tag{7}$$

and

$$\frac{\partial U}{\partial t} + \frac{\partial}{\partial x}\left[\frac{U q_b + U^2 a_1}{A} - \frac{a_1}{b} - \frac{U^2}{2}\right] = 0. \tag{8}$$

The total area is

$$A(x) = a_1 + a_2 = b(1 - h_s). \tag{9}$$

The layer velocities can be recovered from

$$u_1 = \frac{q_b - U a_2}{A} \tag{10}$$

and

$$u_2 = \frac{q_b + U a_1}{A}. \tag{11}$$

Equations (7) and (8) are hyperbolic and have the characteristics

$$c_\pm = \left[\frac{q_b + 2U a_1 - UA}{A}\right] \pm \left[\frac{a_1}{A^2}\left(1 - \frac{a_1}{A}\right)\left(\frac{A}{b} - U^2\right)\right]^{1/2}. \tag{12}$$

These are left and right traveling long interfacial waves relative to the convective velocity given by the first term on the right. Riemann invariants can also be obtained. However, for $U^2 b/A = U^2/(h_1 + h_2) > 1$, the characteristics are complex and (7) and (8) change from hyperbolic to elliptic. This instability is the long-wave limit of the Kelvin–Helmholtz instability. Lawrence (1990) has shown that the stability criterion is violated over some regions for steady exchange flow through a contraction with $|q_b| > 0$, though the criterion is never exceeded at the control points (AF). The growth rate found from (12) is $\mathrm{Im}(c_- k) \sim k$, where k is the horizontal wavenumber. High wavenumbers will grow fastest. This behavior is somewhat spurious since the dynamics of high wavenumbers is beyond the model's region of validity ($k \to 0$). Relaxation of the hydrostatic assumption shows that for any shear U there is always an unstable wavenumber k (Turner 1973). In practice this instability will lead to mixing on small scales. Thus, to control this instability in the present study some dissipation must be added to the model. This is discussed below.

For the cases considered in this paper, the imposed barotropic transport is periodic with zero time mean and given by

$$q_b(t) = q_{b0} \sin\left(2\pi \frac{t}{T}\right), \tag{13}$$

where q_{b0} is the barotropic transport amplitude and T is the period. The barotropic velocity at any point in the channel is $q_b(t)/A(x)$. Rescaling (7) and (8) with

$$\tau = t/T, \quad \xi = x/L$$

gives

$$\frac{\partial a_1}{\partial \tau} + \gamma \frac{\partial}{\partial \xi}\left(\frac{a_1 q_B(\tau) - U a_1 A + U a_1^2}{A}\right) = 0 \tag{14}$$

and

$$\frac{\partial U}{\partial \tau} + \gamma \frac{\partial}{\partial \xi}\left(\frac{U q_b(\tau) + U^2 a_1}{A} - \frac{a_1}{b} - \frac{U^2}{2}\right) = 0. \tag{15}$$

Here $\gamma = T/L$ and L is the lengthscale of the strait. In this study L is taken to be twice the distance from the narrows ($b = 1$) to the point where $b = 2$ for a pure symmetric contraction, and for an offset sill–narrows combination L is the sill to narrows separation distance.

Once the strait geometry is specified, solutions to (13), (14), and (15) depend on just the two nondimensional parameters γ and q_{b0}. In dimensional variables,

$$\gamma = \frac{(g'H)^{1/2} T}{L} \tag{16}$$

and

$$q_{b0} = \frac{u_{b0}}{(g'H)^{1/2}}. \tag{17}$$

Here u_{b0} is the dimensional barotropic velocity where $A = 1$.

The parameter γ is a measure of the length of the strait relative to the distance an internal signal [speed $\sim (g'H)^{1/2}$] will travel in a forcing period. Or γ may be thought of as the distance a particle will travel due to the buoyancy-driven flow alone in a tidal period relative to the strait length. For $\gamma \to \infty$ (a dynamically short strait), the time-dependent terms in (14) and (15) are insignificant and the quasi-steady limit is recovered. When $\gamma \to 0$, the temporal variations are zero and the unforced steady solution (i.e., the initial condition) is unaltered by the forcing. The second parameter q_{b0} is a measure of the strength of the barotropic forcing compared to the buoyancy-driven exchange velocity [$\sim (g'H)^{1/2}$]. Armi and Farmer and FA recognized that for their quasi-steady solutions to be valid $\gamma \gg 1$. The objective here is to quantify this assertion and explore solutions to (14) and (15) with q_b given by (13) as a function of strait geometry, q_{b0}, and γ.

Numerical methods

Since (14) and (15) typically have complex characteristics for the flows considered here, they are most easily solved numerically. The solutions are obtained using the two-step Lax–Wendroft method (Press et al. 1986). This method is second-order accurate in both ξ and τ. It also has the advantage of correctly following the development and propagation of shocks, which may naturally arise in such flows. These equations were solved with a dissipation term $\nu U_{\xi\xi}$, with ν a constant, added to the right-hand side of (15). This form of dissipation follows from assuming a horizontal Laplacian friction ($=\hat{\nu} u_{ixx}$) in each of the layers. This term was included primarily to control growth of the high wavenumbers in regions of unstable shear where the computational grid mode is the most unstable wave. Without dissipation these high wavenumber disturbances grow without saturation and overwhelm the solution. The dissipation effectively models small-scale mixing that would occur throughout the strait and is enhanced in regions of unstable flow. It also reduces the small-scale grid oscillations near shocks, which arise due to the numerical technique. In addition to damping, in the linear limit this term introduces a high wavenumber cutoff of the shear instability. Other, more sophisticated dissipation terms could have been employed; however, they are not any more physically realistic than that used. The objective was just to control the instability without significantly altering the solutions and the average transport.

Evaluation of a set of runs in which only ν varied showed that the dissipation could be maintained small enough to not significantly affect the calculated flow within the strait and the average exchange flow. As will be shown in the next section, this was possible since the instability typically occurred in outflow regions and was quickly swept out of the model domain by the supercritical flow. An estimate of the significance of this dissipation term is the Peclet number $\gamma UL/\nu$. Typically $\gamma \geq 1$, $U \sim 1$, $L \sim 1$, and $\nu = 10^{-3}$ to 10^{-1} giving $\gamma UL/\nu \sim 10$ to 10^3. Even in the most viscous cases on the scales of interest here ($L \sim 1$) the nonlinear terms are an order of magnitude larger than the dissipation, and for most situations are two to three orders of magnitude larger.

For a typical run, variation of ν above the minimum required to obtain a stable solution showed that the calculated average transport changed by less than one-half percent for a factor of two change in ν. Increasing γ or q_{b0} tended to require an increased ν, although for γ increasing this is consistent with the dimensional value of ν held nearly constant. As will be seen in the next section, the unforced steady and forced quasi-steady results could be recovered, suggesting that the role of this dissipation was minor.

A principal objective of this study is to impose barotropic forcing and solve for the resulting time-dependent and average (over one forcing period) exchange flow. This was accomplished using Sommerfeld radiation boundary conditions

$$\phi_\tau - c\phi_\xi = 0$$

at each end of the strait. Here $\phi = a_1$ and U. The phase speed c near the boundaries was calculated according to Orlanski (1976). Supercritical flow in the exit regions helps to ensure that information propagates out of the domain. The boundary conditions did not prevent flushing of one layer from the central region of the strait for large values of q_{b0}. Use of these boundary conditions implies that once fluid from one basin exits at the opposite end of the strait it does not reenter the domain. Thus, the exiting layer tends to a depth given by the steady maximal exchange solution. The boundaries were well removed from the central region of the strait. Runs were repeated with varying domain lengths to guarantee that the boundary locations did not affect the interior region.

3. Model results

a. *Pure contraction*

The first strait geometry considered is a pure contraction with no depth variations ($h_s = 0$). Figure 2 shows the unforced (no barotropic flow) steady maximal exchange hydraulic solution for a symmetric contraction given by

$$b(\xi) = 1 + 4(1 - e^{-\alpha^2\xi^2}). \qquad (18)$$

The origin is at the narrows and $\alpha = 1.073$, $b = 2$ at $\xi = \pm 1/2$. This choice of strait geometry is representative of this class of flows. The time-dependent solutions change quantitatively, but not qualitatively as the strait geometry is modified. In the discussion we consider the consequences of this result. In Fig. 2a the interface position is shown. The upper layer flows from left to

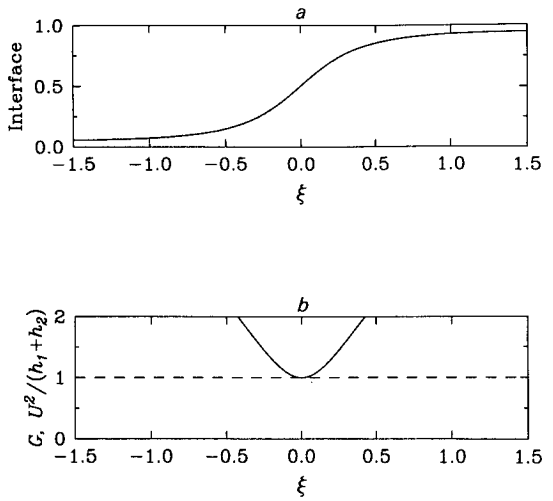

FIG. 2. Unforced steady maximal exchange solution for flow through the contraction given by (18). (a) The interface in the strait. (b) The Froude number G (solid) and the shear stability parameter $U^2/(h_1 + h_2)$ (dashed).

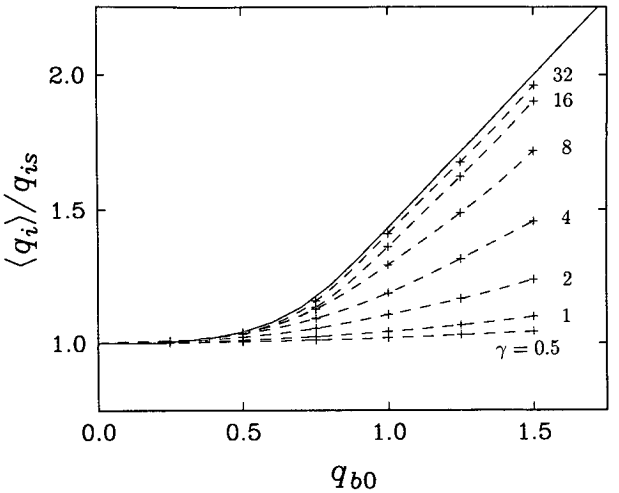

FIG. 3. The average exchange transport $\langle q_i \rangle$, normalized by the unforced steady transport q_{is}, versus the amplitude of the barotropic flow q_{b0} for several values of γ, for the contraction given by (18). The solid curve is the quasi-steady theory.

right. The Froude number $G = 1$ at the narrows and is supercritical everywhere else (Fig. 2b). Also shown in Fig. 2b is the shear parameter $U^2/(h_1 + h_2)$, which is marginally stable throughout the strait. The unforced steady solution gives $u_i = \pm 1/2$ at the narrows and an exchange transport $q_{is} = u_i a_i = \pm 1/4$. The subscript s denotes a unforced steady ($q_b = 0$) layer transport. For the geometry of Fig. 2, u_1 and q_1 are positive and u_2 and q_2 are negative. With a steady barotropic flow the layer opposing the barotropic flow will be arrested for $|q_b| = 0.544$ and expelled from the narrows for $|q_b| \geq 1$ (AF). In the quasi-steady theory with a barotropic forcing given by (13), the exchange transport calculated at the narrows and averaged over a tidal period $\langle q_i \rangle$ increases above the unforced transport for $q_{b0} \geq 0.5$, when the barotropic flow is strong enough to arrest the opposing layer (see Fig. 3 below). Note that since the barotropic forcing has zero mean, $\langle q_2 \rangle = -\langle q_1 \rangle$.

The effect of the time dependence on average transport the geometry of Fig. 2 is shown in Fig. 3, where $\langle q_i \rangle / q_{is}$ is plotted versus q_{b0} for several values of γ. The solid line is the quasi-steady theory from AF. These results were obtained by integrating (14) and (15) with $q_b(\tau)$ given by (13) and the unforced steady solution as the initial condition. The calculations were run until a periodic solution developed. Although the system is highly nonlinear, periodic solutions always developed after just two or three forcing periods. Initial conditions different from the unforced steady solution adjusted to the steady solution with no forcing and to the same periodic solutions when forcing is applied. For fixed γ, $\langle q_i \rangle$ increases as q_{b0} increases. For fixed q_{b0}, $\langle q_i \rangle$ increases as γ increases until the quasi-steady result is approached. These calculations show that the quasi-steady theory ($\gamma \to \infty$) gives an upper bound on the average exchange and the unforced steady exchange ($\gamma \to 0$) gives a lower bound. Only when $\gamma \gtrsim 30$ does the quasi-steady theory become a good approximation. Thus the strait must be dynamically very short in the

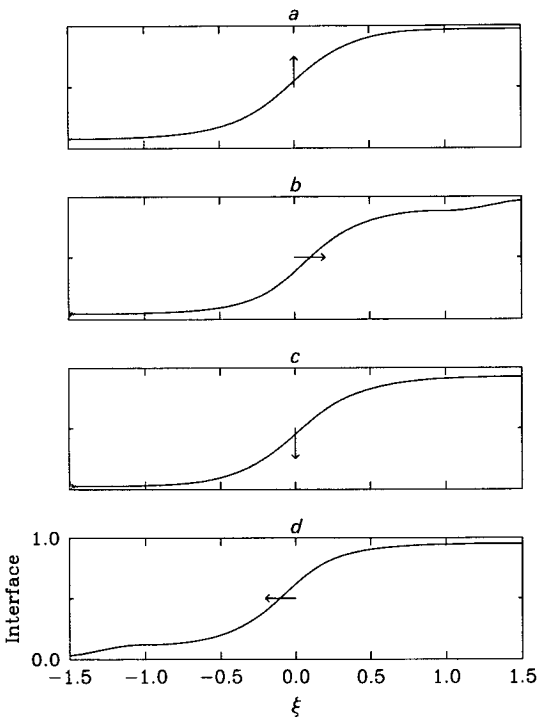

FIG. 4. Solution of (14) and (15) for the pure contraction for $\gamma = 4$ and $q_{b0} = 0.5$ at four points through the forcing period after the periodic solution is obtained. Time increases from (a) to (d). The arrow indicates the phase and direction of the barotropic flow.

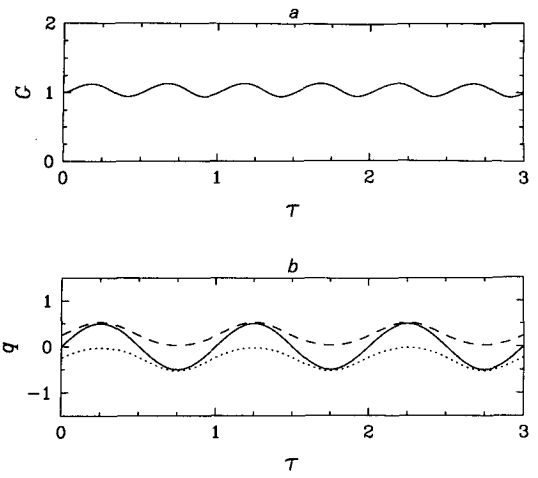

FIG. 5. (a) The Froude number G at the narrows for the run in Fig. 4. (b) The layer transports q_1 (dashed) and q_2 (dotted) and the barotropic transport q_b (solid) versus τ.

sense implied by (16) for the quasi-steady theory to be an acceptable approximation.

In Fig. 4 the interface evolution over a forcing cycle, after the periodic solution is obtained, is shown for the case $\gamma = 4$ and $q_{b0} = 0.5$. The rotating arrow indicates the phase of the barotropic flow (measured clockwise from the vertical). For these parameters the forcing is relatively weak, and there is little effect on the average transport (see Fig. 3). The interface moves back and forth with the barotropic flow but is still similar in shape to the steady solution. The interface height at the narrows lags slightly behind the barotropic flow. In Figs. 4b (4d), there is a small amplitude surge of upper (b) [lower (d)] layer fluid, which moves out of the strait as the barotropic forcing relaxes.

In Fig. 5a, G at the narrows is shown as a function of time for the run in Fig. 4. The periodic solution is obtained almost immediately. Here G oscillates nearly sinusoidally around $G = 1$ with a frequency twice that of the forcing. In Fig. 5b, the layer transports q_i at the narrows and the barotropic flow q_b are shown. For low q_{b0} the layer transports never reverse and the response is nearly sinusoidal.

The effect on the evolution of increasing the forcing strength is shown in Fig. 6, where $\gamma = 4$ and $q_{b0} = 1$. Again the solution has reached the periodic state. For this barotropic amplitude the steady theory predicts that the opposing layer will just be pushed from the narrows. As the tidal flow increases from left to right (Figs. 6a,b,c) the lower layer is nearly expelled from the narrows. Reversal of the barotropic flow (Figs. 6c,d,a) releases the lower layer. It then forms a bore, or density current, reminiscent of the head of a density current formed from the sudden removal of a barrier, that propagates through the strait. By symmetry the process repeats for the upper layer on the opposite phase of the forcing. It is just behind the head of the

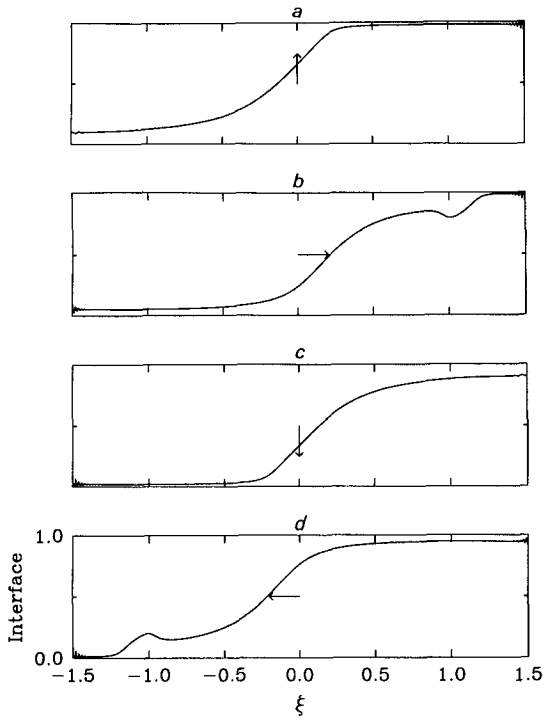

FIG. 6. Solution for the pure contraction with $\gamma = 4$ and $q_{b0} = 1.0$ at four points through the forcing cycle.

surge that the shear instability develops most rapidly. The damping term becomes significant locally and is necessary to control the growth of the high wavenumbers (remnants of which are visible near the boundaries). This localized damping is not unreasonable since it is known that the heads of density intrusions are regions of intense mixing and dissipation (Simpson 1982).

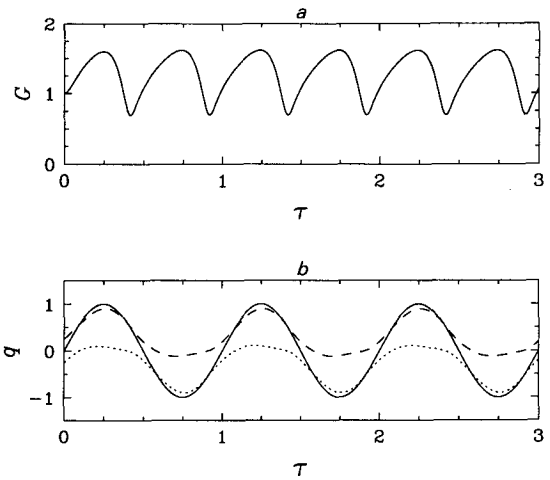

FIG. 7. (a) G at the narrows for the run in Fig. 6; (b) q_1 (dashed) and q_2 (dotted) and q_b (solid) at the narrows.

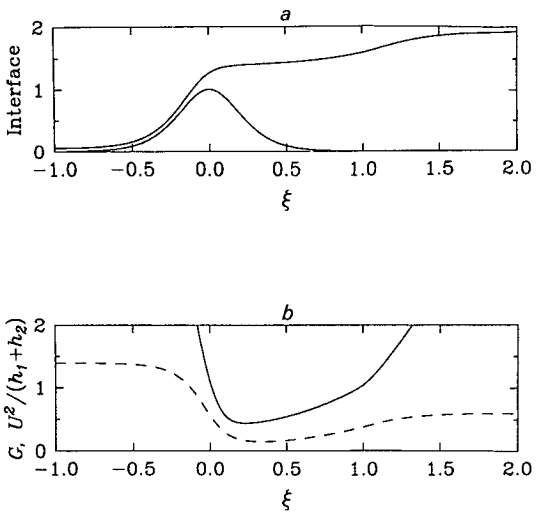

FIG. 8. Unforced steady maximal exchange solution for the sill–narrows combination given by (19) and (20). (a) The sill and interface; (b) G (solid) and $U^2/(h_1 + h_2)$ (dashed).

Figure 7a shows the Froude number at the narrows as a function time. The flow is never controlled in the sense implied by the steady or quasi-steady theories since $G = 1$ only instantaneously. The amplitude of the variations in G are increased, and the response departs from the near-sinusoidal behavior found for $q_{b0} = 0.5$. The layer transports q_i at the narrows and q_b are shown in Fig. 7b. The transports (i.e., layer velocities) are reversed during a significant portion of each tidal cycle. The instantaneous transport becomes very pulsed in nature. A further increase of q_{b0} leads to zero transport in each layer during a portion of the tidal cycle as the layer depths are temporarily reduced to zero on the upstream side and at the narrows. Increasing γ tends to stiffen the interface response and leads to larger vertical excursion of the interface. Examples of this effect are shown in the next section.

b. *Offset sill and narrows*

The combination of an offset sill and narrows is slightly more complicated than a pure contraction. It is also more realistic since most straits also have one or more sills. Figure 8 shows the steady maximal exchange solution for a strait with

$$b(\xi) = \frac{1}{2} + \frac{3}{2}(1 - e^{-\alpha^2(\xi-1)^2}) \qquad (19)$$

and

$$h_s(\xi) = 1 - \operatorname{sech}^2\beta\xi. \qquad (20)$$

Here $\xi = 0$ at the sill crest where $b = 1$ and $\xi = 1$ at the narrows where $b = 1/2$. Also $\alpha = 0.637$ for $\xi \leqslant 1$, $\alpha = 1.273$ for $\xi \geqslant 1$, and $\beta = 3.75$. The ratio of the width at the narrows to the width at the sill $B = 1/2$ and the maximum depth is 2. Again, particular choice of parameters is not significant; they are just representative of this type of geometry. The solutions discussed below change quantitatively, but not qualitatively, as the strait geometry is modified.

Figure 8a shows the unforced steady solution interface position throughout the strait. The sill is also shown. The upper layer is again flowing from left to right. The Froude number G and the stability parameter $U^2/(h_1 + h_2)$ are plotted in Fig. 6b. The Froude number is critical at the sill crest and the narrows with subcritical flow between; $G > 1$ outside of this central region. The shear is supercritical only where the lower layer descends down the sill. The unforced steady transport $q_{is} = 0.137$. Over the sill $u_2 = -0.271$ and $u_1 = 0.646$ at the narrows. For steady barotropic flows $q_b \geqslant 0.27$ will arrest the lower layer and $q_b \leqslant 0.65$ will arrest the upper layer. Farmer and Armi (1986) discuss these steady solutions in detail.

As in the previous section, time-dependent solutions with $q_b(\tau)$ given by (13) were calculated for the geometry given by (19) and (20), with the unforced steady solution as the initial condition. In Fig. 9 the average exchange transport $\langle q_i \rangle / q_{is}$ is again plotted versus q_{b0} for several values of γ. The quasi-steady result from FA for $B = 1/2$ is also shown. The results are qualitatively the same as the pure contraction case. Increasing γ for fixed q_{b0} increases the average exchange. The limits $\gamma \to \infty$ and $\gamma \to 0$ give the maximum and minimum exchanges, respectively. For the quasi-steady approximation to be valid, γ must again be greater than about 30. There are greater variations in $\langle q_i \rangle$ for $q_{b0} < 0.5$ than in the pure contraction case. This result is due to the geometrical asymmetry and magnitudes of the unforced steady solution layer velocities at the two control points.

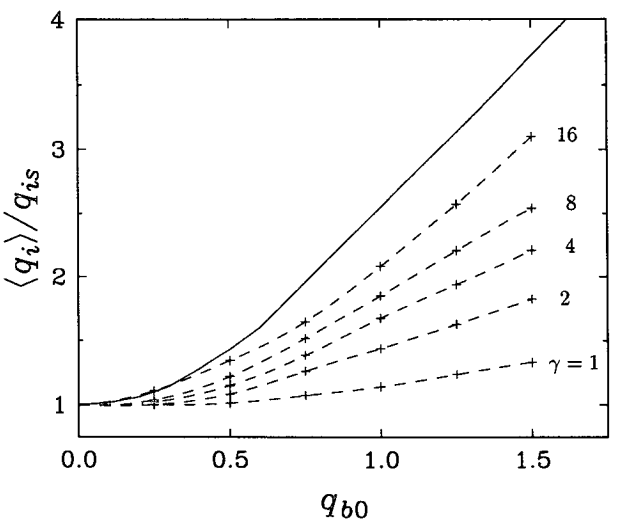

FIG. 9. Normalized average exchange transport $\langle q_i \rangle / q_{is}$ versus q_{b0} for several values of γ for the sill–narrows combination given by (19) and (20). The solid curve is the quasi-steady theory.

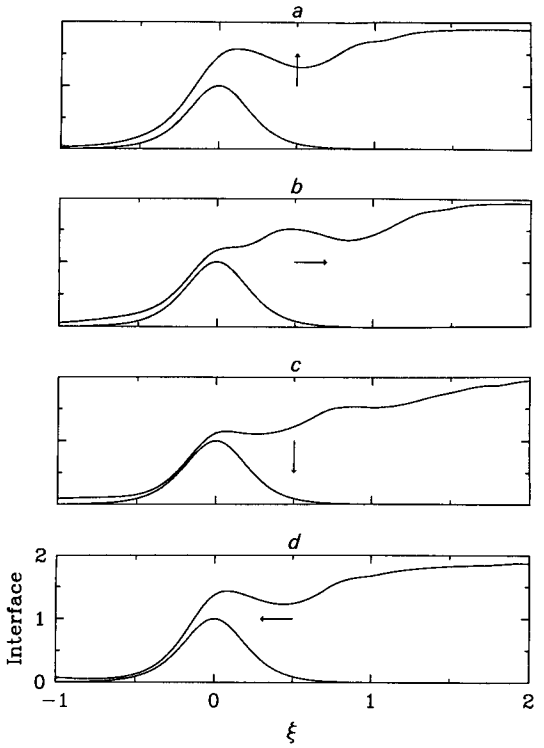

FIG. 10. Solution for the sill–narrows case with $\gamma = 1$ and $q_{b0} = 1$ at four times throughout the forcing cycle.

An example of the evolution of the flow within the strait is shown in Fig. 10 for $\gamma = 1$ and $q_{b0} = 1$. The figures are from after the development of the periodic solution. The interface descends nearly to the sill crest and upper layer between the sill and the narrows is deepened as the barotropic tide is converted to an internal signal. On the opposite phase of the tide (Figs. 10c,d,a), the interface is pushed back up and the lower-layer flow over the sill is increased. This correlation of layer velocity with layer depth agrees with the Candela et al. (1990) observations at Gibraltar.

The evolution of G at the sill and the narrows is plotted in Fig. 11a for the run in Fig. 10. At the sill G remains near one when the barotropic flow is into the strait. Reversal of the barotropic flow causes G to greatly increase. A similar pattern occurs at the narrows with G nearer to one on the incoming tide than on the outgoing phase. This pattern is due to internal waves generated within the strait that are swept through the narrows or over the sill on the respective outgoing phase of the forcing. Figures 10b and 10c show the layer transports at the sill and narrows. At the sill the upper layer displays the largest variations, while at the narrows the lower-layer transport is more variable. At both the sill and the narrows, both layers are reversed during portions of the forcing cycle. The reversal is most pronounced for the upper layer over the sill and the lower layer at the narrows.

The result of increasing γ is shown in Fig. 12 where $\gamma = 4$ and $q_{b0} = 1$. The left to right phase of the barotropic flow forces the interface to drop down onto the sill upstream and over the crest (Figs. 12a,b,c). The upper layer between the sill and narrows becomes thicker than the corresponding time in Fig. 10. As the tide reverses (Figs. 12c,d,a) the interface over the sill rises sharply, forming a buldge of upper-layer fluid between the sill and narrows that begins to develop into a shock. As the tide begins to flow from left to right, the pulse decays and propagates out of the strait.

The Froude number at the sill and narrows is plotted in Fig. 13a. Again there is significant variability in G, but there are extended periods when $G \approx 1$ both at the sill and the crest. The transports are shown in Fig. 13b and 13c. At the sill q_2 is zero over much of the forcing period. Outflow over the sill occurs as periodic pulses. The transport in the upper layer at the narrows drops sharply as the shock moves through the narrows.

4. Laboratory experiments

a. Method

Laboratory experiments were conducted and compared with the time-dependent theory for the pure contraction geometry. The experimental setup follows the methods employed by Stigebrandt (1977), except

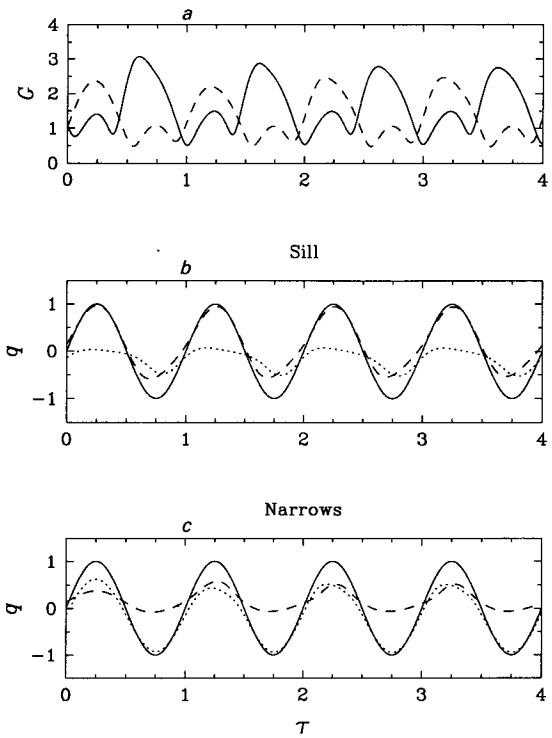

FIG. 11. (a) G at the sill (solid) and the narrows (dash) for the run in Fig. 10. The barotropic q_b (solid) and layer transports q_1 (dash) and q_2 (dotted) at (b) the sill and (c) the narrows.

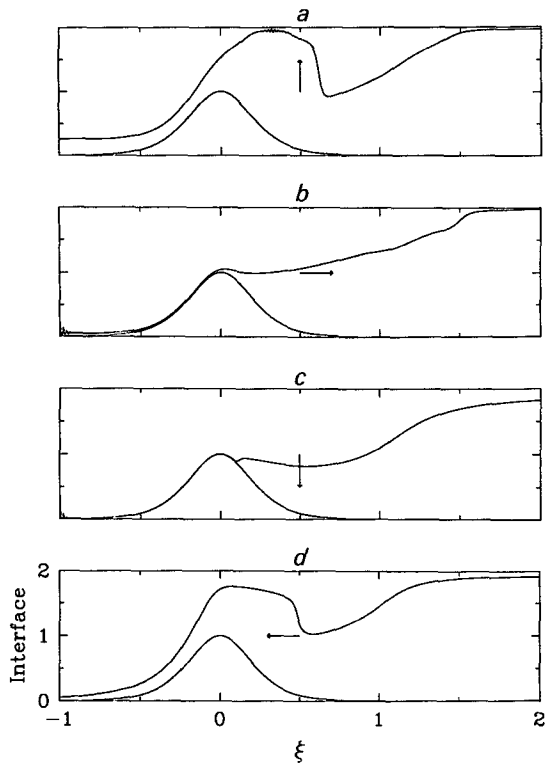

FIG. 12. Solution for the sill–narrows case with $\gamma = 4$ and $q_{b0} = 1$.

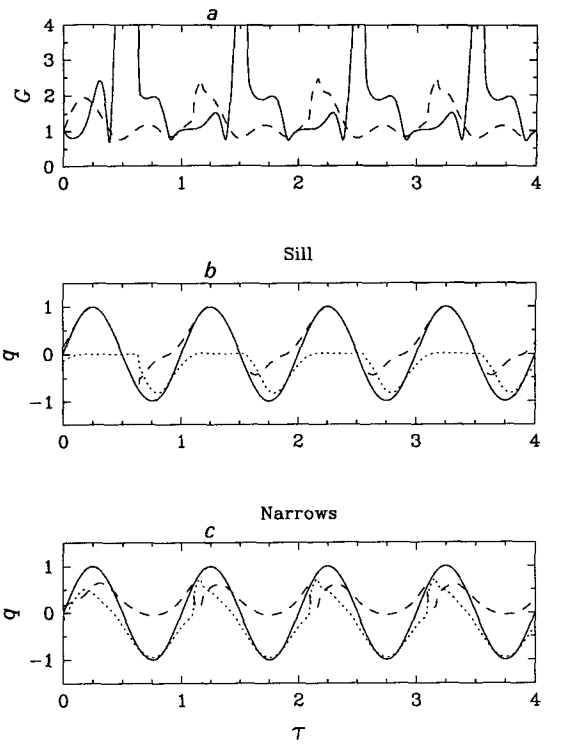

FIG. 13. (a) G at the sill (solid) and the narrows (dashed) for the run in Fig. 12. The transports q_b (solid), q_1 (dashed), and q_2 (dotted) at (b) the sill and (c) the narrows.

here the strait is of finite length rather than zero length ($\gamma \to \infty$). This permits the role of the time-dependent parameter γ to be examined.

A sketch of the experimental setup is given in Fig. 14. A small tank (50 cm × 50 cm × 25 cm deep) was suspended in a larger (200-cm diameter) tank. A symmetric contraction attached to the small tank connected the two "basins." The strait was given by (in dimensional variables)

$$b(x) = b_0\left[1 + 4\left(\frac{x}{L}\right)^2\right], \quad |x| \leq \frac{L}{2},$$

where $x = 0$ is at the narrows. Straits with lengths $L = 10$, 20, 30, and 40 and $b_0 = 5$ cm were used.

Saltwater with density ρ_1 in the small tank and density $\rho_2 (> \rho_1)$ in the large basin was separated by a gate. Removal of the gate initiated an exchange flow. A barotropic oscillation was superimposed on the buoyancy-driven exchange by vertically oscillating the small tank and strait with a displacement $z = a_0 \sin(2\pi t/T)$. After eight or more forcing periods the gate was replaced and the fluid in the small basin was completely mixed. The average exchange flow $\langle q_i \rangle$ was calculated from the salt (density) flux into the small tank,

$$\langle q_i \rangle = \frac{V_B}{T_G}\left(\frac{\rho_{1f} - \rho_1}{\rho_2 - \rho_1}\right), \tag{21}$$

where V_B is the total volume of fluid within the small tank, T_G is the time the gate was removed, and ρ_{1f} is the density in the small tank after mixing. The depth of the small tank and the size of the exterior tank min-

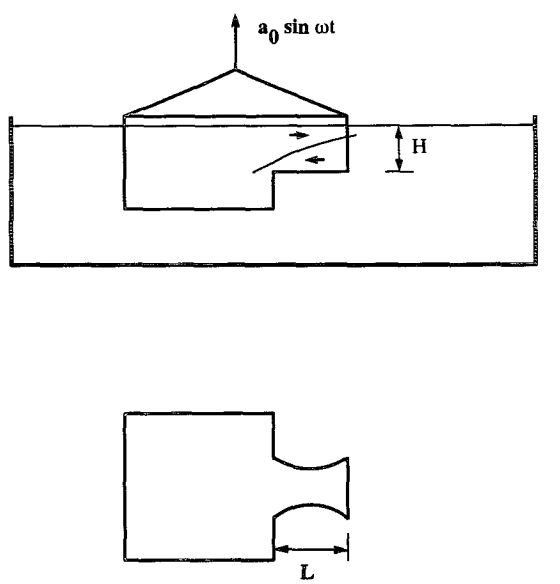

FIG. 14. Experimental setup.

imized reentry of fluid into the strait once it had traversed the strait.

Large barotropic flows were achieved by forcing at frequencies near the Helmholtz frequency of the system. This allowed barotropic velocities at the narrows u_{b0} of up to 25 cm s^{-1} for oscillation amplitudes $a_0 \leq 0.3$ cm. For a given L, T, and a_0, u_{b0} was measured for a homogeneous flow ($\rho_1 = \rho_2$) using an impellor current meter (Nixon Streamflo Model 401) positioned in the narrows at middepth. This device consists of a 1-cm diameter impellor suspended in the flow by a 0.3-cm diameter shaft. The impellor spin frequency was measured and converted to velocity via a calibration chart. Although q_{b0} (i.e., u_{b0}) was found for homogenous flow, the barotropic forcing will not be significantly different with a superimposed buoyancy-driven flow because of the very small density differences used.

The parameter values investigated were L = 10, 20, 30, and 40 cm; b_0 = 5 cm; H = 9 cm; $(\rho_2 - \rho_1)/\rho_2 < 0.01$; T = 10–15 s; and $u_{b0} \leq 25$ cm s^{-1}. Thus, the experiment investigated the ranges $1 \leq \gamma \leq 11$ and $0 \leq q_{b0} \leq 2.5$. Errors in measured $\langle q_i \rangle$ were due primarily to the resolution of the density measurements. A precision electronic densiometer that measures density to 10^{-4} g cm^{-3} was used. Typically, in (21) $(\rho_{1f} - \rho_1) = 0.0020$ gm cm^{-3} and $(\rho_2 - \rho_1) = 0.0100$ gm cm^{-3}, giving a maximum uncertainty of $\pm 10\%$ in $\langle q_i \rangle$. The measurements of u_{b0} were accurate to ± 1 cm s^{-1}, leading to an uncertainty in q_{b0} of about $\pm 10\%$.

The Reynolds number $u_i H/\nu \approx 4000$ for typical values $u_i \sim 4$ cm s^{-1}, H = 9 cm, and kinematic viscosity $\nu = 0.01$ cm^2 s^{-1}. This is large enough so that viscous effects do not dominate the flow. Viscous sidewall and bottom boundary layers in the straits have a maximum thickness $(\nu L/u_i)^{1/2} \approx 0.3$ cm for $u_i = 4$ cm s^{-1} and L = 40 cm. The boundary layers occupy only a small fraction (<5%) of the layer depths. The interfacial boundary layer is turbulent and, as discussed below, this is important in interpreting the results. Departures from the hydrostatic assumption ($H/L \ll 1$) are significant since $H/L = 1/4 - 1$. However, steady hydraulic theory is known to work well even when the hydrostatic approximation is violated (Henderson 1966).

b. Results

A direct comparison of the experiment and theory for interface position throughout the strait as a function of forcing phase is shown in Fig. 15 for a run with $\gamma = 7.8$ and $q_{b0} = 1$. Time dependence is important and the forcing is strong. The figure shows side view photographs of the strait. The dyed upper-layer fluid is flowing, on average, from left to right. This run used the 20-cm long strait. Shown to the left of each photograph are the interface shapes calculated with the model using the experimental parameters. The agreement throughout the forcing cycle is quite good. The largest differences occur when the model predicts layer depths approaching zero. This disagreement is probably due to viscous boundary layers and to the reentry of some fluid back into the strait that could not be entirely avoided for large q_{b0} in the experiments. The experiments show clear indications of interfacial mixing occurring throughout the strait over the entire forcing cycle. This mixing is important in assessing the measured transports and is discussed below. The generally good agreement in the figure also supports the use of a hydrostatic model, even for these time-dependent flows with relatively large aspect ratios. In this experimental run $H/L = 0.45$.

Figure 16 shows the measured exchange $\langle q_i \rangle$, normalized by the theoretical unforced steady exchange q_{is}, plotted versus q_{b0}. Each symbol type corresponds to a specific L, though γ varies among runs with L fixed. The dashed lines are the experimentally derived contours of constant γ. The contours were drawn by inspection but are not significantly different from contours obtained by more sophisticated techniques. They are consistent with the experimental uncertainty. The solid circles are the data from Stigebrandt's (1977) experiments, which correspond to $\gamma \to \infty$. The experiments and model results (cf. Fig. 3) agree qualitatively. The most obvious quantitative difference between experiment and theory is the lower measured transports for all γ and q_{b0} than predicted by the model. Also, for a given γ, $\langle q_i \rangle$ does not increase as rapidly at the model predictions. Stigebradt's (1977) data give the largest transports, but they are also below the quasi-steady theory (the solid line).

This overall reduction in measured transport, when compared to the model, may be primarily due to interfacial mixing, which was observed to occur in all experimental runs. Formation of a finite thickness interface by mixing between the two uniform layers will reduce the salt transport from the theoretical prediction. An estimate of the magnitude of this effect for steady flow with no barotropic flow can be made following Anati et al. (1977). It is assumed that an interface of thickness δ develops in which velocity and density vary linearly between their theoretical uniform values u_i and ρ_i (i = 1, 2). Koop and Broward (1979) showed that the bulk Richardson number for fully developed stratified shear layers is $g'\delta/(u_2 - u_1)^2 \approx 0.3$, or $\delta \approx 0.3(u_2 - u_1)^2/g'$. For a pure contraction $u_2 - u_1 = (g'H)^{1/2}$ throughout the strait, giving $\delta \approx 0.3\,H$.

The density (or salt) transport through the strait is (in dimensional variables)

$$F_\rho = b \int_0^H \rho(z)u(z)dz, \tag{22}$$

where $\rho(z)$ and $u(z)$ and density are velocity with depth z. Evaluating (22), assuming linear variations of u and ρ between u_1 and u_2 and ρ_1 and ρ_2, across the interface of thickness δ gives

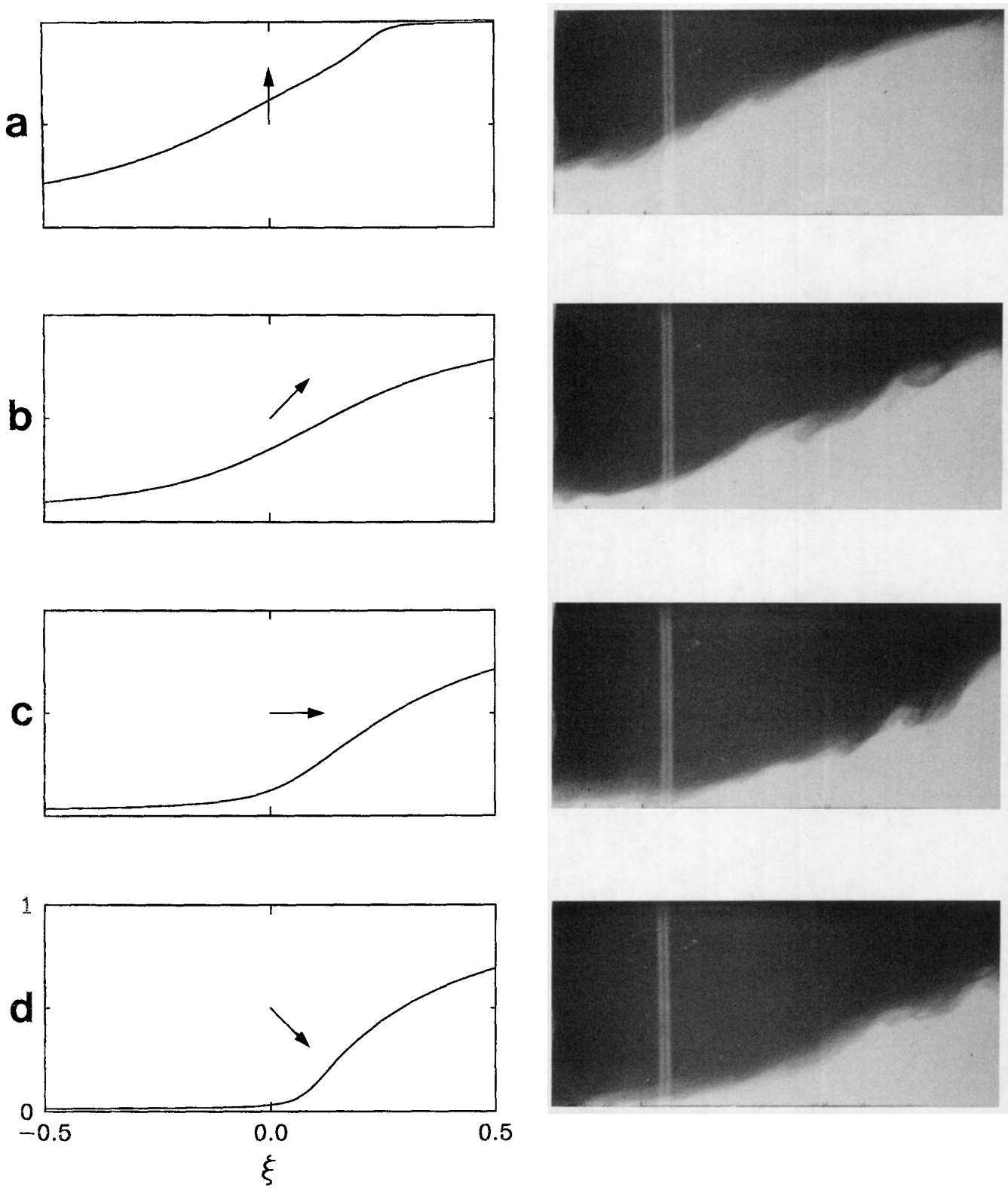

FIG. 15. Comparison of model and experimental interface positions in the strait over a forcing period for a run with $\gamma = 7.8$ and $q_{b0} = 1.0$. Time increases from (a) to (h). The arrow indicates the phase of the forcing.

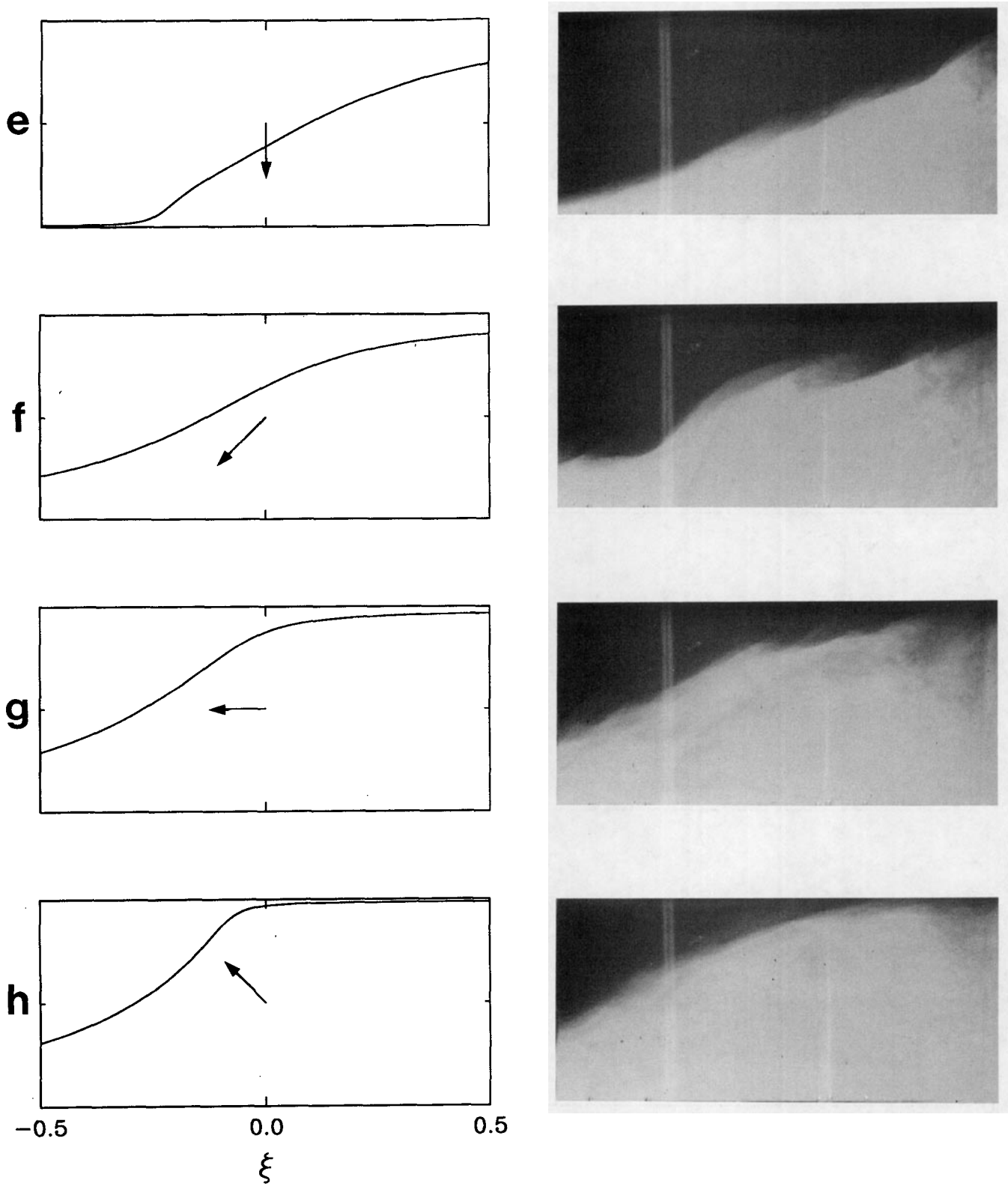

FIG. 15. (*Continued*)

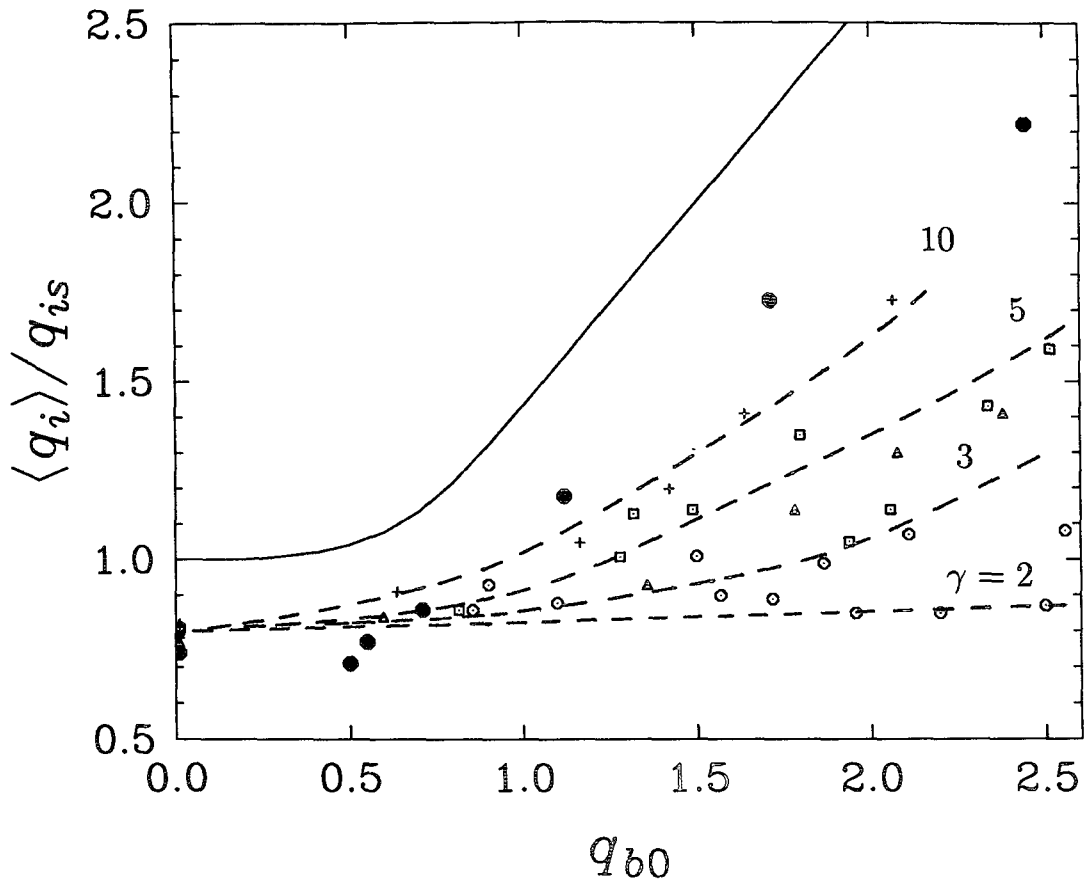

FIG. 16. Exchange transports $\langle q_i \rangle$, normalized by q_{is}, vs q_{b0} from the laboratory experiments. The dashed lines are contours of γ = 2, 3, 5, and 10 derived from the experiments. Each symbol corresponds to a run with a strait of L = 10 cm (+), 20 cm (□), 30 cm (△), 40 cm (○); γ varies among runs with a constant L. The solid circles are the data from Stigebrandt (1977) and correspond to $\gamma \to \infty$.

$$F_\rho = (\rho_2 - \rho_1) q_{is} \left(1 - \frac{2}{3}\frac{\delta}{H}\right) \approx 0.8(\rho_2 - \rho_1) q_{is}$$

for $\delta \approx 0.3\ H$ and $q_{is} = \frac{1}{4} b_0 g'^{1/2} H^{3/2}$.

The estimate of volume transport used in the experiment (21) is $F_\rho/(\rho_2 - \rho_1)$. Thus, salt transport after accounting for mixing should be approximately $0.8 q_{is}$, in good agreement with the experimental results for $q_{b0} = 0$. A mixing layer model with a hyperbolic tangent profile for $u(z)$ and $\rho(z)$ and a Richardson number of 1/4 gives a salt transport of $0.75(\rho_2 - \rho_1) q_{is}$. These estimates of the magnitude of the mixing effect show that volume transport estimates obtained from salt exchange should be below the steady theoretical prediction. For runs with time-dependent barotropic forcing the mixing is modulated both spatially and temporally, but the average effect is still to reduce the average salt transport. If, as a first-order estimate, all the measured transports are renormalized with $0.8 q_{is}$ instead of q_{is}, then better quantitative agreement with the theory is obtained.

5. Discussion

The steady theory of two-layer hydraulic exchange flows has been extended to include time dependence and forcing by a barotropic tidal flow. The model demonstrates the significance of two parameters, γ (16), which measures the importance of time-dependence, and q_{b0} (17), which measures the strength of the barotropic forcing. For both a pure contraction and an offset sill–narrows combination the average exchange increases with increasing q_{b0} for a given γ. For a fixed q_{b0} the transport increases with increasing γ. The minimum exchange for any q_{b0} is given by the unforced steady maximal exchange and obtained when $\gamma \to 0$. For $\gamma \to \infty$ the exchange approaches a maximum equal to the quasi-steady result of AF and FA.

This qualitative behavior is independent of the details of the geometry of the strait. However, with the addition of time dependence and periodic forcing the geometric details of the complete strait, not just geometric conditions at the steady control points, are necessary to determine the exchange. To illustrate this

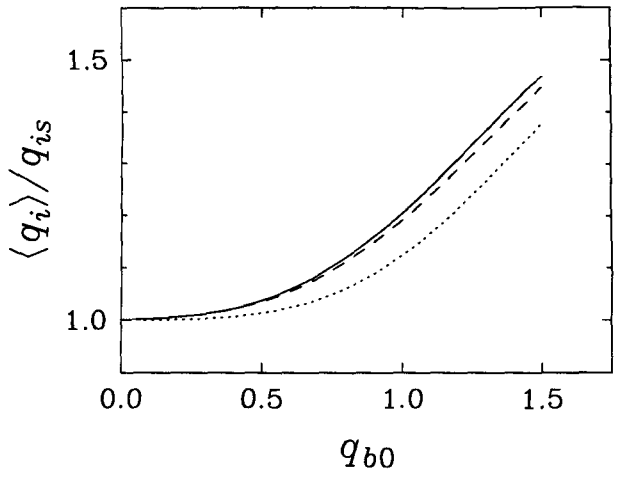

FIG. 17. The normalized average transport for three straits given by Eq. (18), solid; (23), dashed; and (24), dotted. All three curves were calculated for $\gamma = 4$.

point the average transport for three pure contractions as functions of q_{b0} with $\gamma = 4$ was computed. One strait is given by (18), and the other two are given by

$$b(\xi) = 1 + 4\xi^2 \tag{23}$$

and

$$b(\xi) = 1 + 8|\xi^3|. \tag{24}$$

All three have the same minimum width and L and therefore the same q_{is}. Also the average layer velocity from the steady solutions between $\xi = -1/2$ and $1/2$ is the same in all three cases. Figure 17 shows that each strait gives a different average transport for a given q_{b0}. From this, it can be inferred that one could reduce the minimum width of a strait yet retain the same transport by altering the other details of the geometry of the strait. This argues against the usual concept of hydraulic control based on a few critical geometric parameters as occurs in the steady and quasi-steady theory. The steady control points only provide a weak control on the transport in that they give the minimum and maximum bounds.

The laboratory experiments support the model results but also highlight the significance of mixing in real fluids. Since salt, or heat, transport is often the quantity of oceanographic interest the issue of mixing is critical. The simple, steady mixing layer model presented here indicates that the salt flux is reduced about 20% below the steady two-layer model predictions. The spatial and temporal dependence of mixing is unresolved. Geyer and Cannon (1982) have observed large temporal variations in mixing associated with tidal forcing of flow at the entrance sill to Puget Sound. This is an issue that needs further work because of the effect on salt transport and also because the formation of a mixed layer throughout the strait moves the dynamics away from the assumption of two uniform layers.

A potentially significant deficiency of this and all hydraulic models is that they are hydrostatic. Important features, such as internal solitary waves and resonant wave generation by flow over topography (Grimshaw and Smyth 1986; Melville and Helfrich 1987), are not captured. Kinder (1984) has shown that as much as 40% of the transport of Atlantic water through the Strait of Gibraltar occurs as large amplitude internal undular bores periodically formed by the release of the hydraulic jump downstream of Camirinal Sill. The hydraulic models do admit shocks, which are the nondispersive limits of the undular bores and solitary waves. The initial evolution of these dispersive waves should be well modeled by a hydrostatic theory. At longer times dispersion will become important. While some aspects of wave evolution may be inadequately modeled, the overall effect on the average transport should be small.

The time-dependent model demonstrated that there is a broad region of parameter space, $\gamma = O(1)$, where time dependence must be considered when estimating the average exchange through a strait. A survey of some oceanic straits shows that many fall into this parameter range. Table 1 lists some straits and estimated values of γ and q_{b0}. These straits are all relatively narrow so that rotational effects should be small. Values of $\gamma = O(1)$ are common. No attempt has been made to calculate a transport for each strait, but what is clear is that many will be incorrectly modeled with an unforced steady or quasi-steady hydraulic theory.

As a specific example consider the Strait of Gibraltar. Assuming that Camirinal Sill and Tarifa Narrows are the steady control points $H = 280$ m, $L = 20$ km,

TABLE 1. Values of γ and q_{b0} for some straits.

Strait	g' (m s^{-2})	H (m)	L (km)	γ	q_{b0}	Source
Gibraltar	0.02	280	20	5.3	0.6	Armi and Farmer (1988)
Messina	0.01	80	10	4.0	2	Bignami and Salusti (1990)
Bosphorous	0.12	35	30	3.1	0.25	Ünlüata et al. (1990)
Oslofjord	0.02	15	10	2.5	1	Stigebrandt (1977)
Lombok	0.05	350	40	4.7	0.5	Murray et al. (1990)
Tiran	0.0035	270	3	15	0.25	Murray et al. (1984)
Bab-el-Mandeb	0.015	185	130	0.5	0.3	Defant (1961)

$g' = 0.02$ m s^{-2}, and $T = 4.5 \times 10^4 s$, giving $\gamma = 5$. The barotropic velocity over the sill $u_{b0} \approx 1.25 - 1.5$ m s^{-1}, depending on the phases of the tidal components (Candela et al. 1990), giving $q_{b0} \approx 0.6$. The width ratio $B = 1/2$. For these values the quasi-steady theory shown in Fig. 8 gives $\langle q_i \rangle / q_{is} = 1.6$. The geometry used to compute the time-dependent transports Fig. 8 is not the precise Gibraltar geometry but is similar enough to give a reasonable estimate. With $\gamma = 5$, Fig. 8 gives $\langle q_i \rangle / q_{is} = 1.2$ for the q_{b0} range above. This transport is still larger than the observations ($\langle q_i \rangle / q_{is} \leq 1$), but is better than the quasi-steady result. If a first-order estimate for the effects of mixing is to reduce the transport by 20%, then $\langle q_i \rangle / q_{is} \approx 0.95$, in good agreement with the observations. Garrett et al. (1990) have argued that Gibraltar is in a submaximal state (i.e., the control at Tarifa narrows is flooded, $G < 1$). This would also reduce the transport. However, this effect has not been considered here. The open boundary conditions used in this model lead to maximal exchange. Other effects such as friction, departure from hydrostatics, and rotation may be important, but the simple estimates of the role of time dependence and mixing help to explain the Gibraltar observations.

Acknowledgments. William Morrison assisted with the experiments. This research was sponsored by NSF (OCE-9022088) and ONR (N00014-93-1-0263).

REFERENCES

Anati, D. A., G. Assaf, and R. Thompson, 1977: Laboratory models of sea straits. *J. Fluid Mech.*, **81**, 341–351.

Armi, L., and D. Farmer, 1986: Maximal two-layer exchange through a contraction with barotropic net flow. *J. Fluid Mech.*, **164**, 27–51.

——, and ——, 1988: The flow of Mediterranean water through the Strait of Gibraltar. *Progress in Oceanography*, Vol. 21, Pergamon, 1–105.

Bignami, F., and E. Salusti, 1990: Tidal currents and transient phenomena in the Strait of Messina: A review. *The Physical Oceanography of Sea Straits*, NATO/ASI Series, Kluwer Academic, 95–129.

Bryden, H. L., and T. H. Kinder, 1990: Steady two-layer exchange through the Strait of Gibraltar. *Deep-Sea Res.*, **38**(Suppl. 1), 5445–5463.

——, J. C. Candela, and T. H. Kinder, 1994: Exchange through the Strait of Gibraltar, *Progress in Oceanography*, Vol. 33, Pergamon, 201–248.

Candela, J., D. Winant, and A. Ruiz, 1990: Tides in the Strait of Gibraltar. *J. Geophys. Res.*, **95**(C5), 7313–7335.

Defant, A., 1961: *Physical Oceanography*. Vol. 1. Pergamon, 729 pp.

Farmer, D., and L. Armi, 1986: Maximal two-layer exchange over a sill and through the combination of a sill and contraction with barotropic flow. *J. Fluid Mech.*, **164**, 53–76.

——, and ——, 1988: The flow of Atlantic water through the Strait of Gibraltar. *Progress in Oceanography*, Vol. 21, Pergamon, 1–105.

Garrett, C., M. Bormans, and K. Thompson, 1990: Is the exchange through the Strait of Gibraltar maximal or submaximal? *The Physical Oceanography of Sea Straits*, L. J. Pratt, Ed., NATO/ASI Series, Kluwer Academic, 271–294.

Geyer, W. R., 1990: Time-dependent, two-layer flow over a sill. *The Physical Oceanography of Sea Straits*, L. J. Pratt, Ed., NATO/ASI Series, Kluwer Academic, 421–432.

——, and G. A. Cannon, 1982: Sill processes related to deep water renewal in a fjord. *J. Geophys. Res.*, **87**, 7985–7996.

Grimshaw, R., and N. Smyth, 1986: Resonant flow of a stratified fluid over topography. *J. Fluid Mech.*, **169**, 429–464.

Henderson, F. M., 1966: *Open Channel Flow*, Macmillan, 522 pp.

Kinder, T. H., 1984: Net mass transport by internal waves near the Strait of Gibraltar. *Geophys. Res. Lett.*, **11**, 987–990.

Koop, C. G., and F. G. Browand, 1979: Instability and turbulence in a stratified fluid with shear. *J. Fluid Mech.*, **93**, 135–159.

Lawrence, G., 1990: On the hydraulics of Boussinesq and non-Boussinesq two-layer flows. *J. Fluid Mech.*, **215**, 457–480.

Melville, W. K., and K. R. Helfrich, 1987: Transcritical two-layer flow over topography. *J. Fluid Mech.*, **178**, 31–52.

Murray, S. P., A. Hecht, and A. Babcock, 1984: On the mean flow in the Tiran Strait in winter. *J. Mar. Res.*, **42**, 265–287.

——, D. Arief, J. C. Kindle, and H. E. Hurlburt, 1990: Characteristics of the circulation in an Indonesian archipelago strait from hydrography, current measurements and modeling results. *The Physical Oceanography of Sea Straits*, NATO/ASI Series, Kluwer Academic, 3–24.

Orlanski, I., 1976: A simple boundary condition for unbounded hyperbolic flows. *J. Comput. Phys.*, **21**, 251–269.

Press, W. H., B. P. Flannery, S. A. Teukolsky, and W. T. Vetterling, 1986: *Numerical Recipes*. Cambridge University Press, 818 pp.

Simpson, J. E., 1982: Gravity currents in the laboratory, atmosphere, and ocean. *Ann. Rev. Fluid Mech.*, **14**, 213–234.

Stigebrandt, A., 1977: On the effect of barotropic current fluctuations on the two-layer transport capacity of a construction. *J. Phys. Oceanogr.*, **7**, 118–122.

Turner, J. S., 1973: *Buoyancy Effects in Fluids*. Cambridge University Press, 368 pp.

Ünlüata, Ü., T. Oğuz, M. A. Latif, and E. Özsoy, 1990: On the physical oceanography of Turkigh Straits. *The Physical Oceanography of Sea Straits*, L. J. Pratt, Ed., NATO/ASI Series, Kluwer Academic, 25–60.

Wang, D.-P., 1989: Model of mean and tidal flows in the Strait of Gibraltar. *Deep-Sea Res.*, **36**, 1535–1548.